Letter

Hilbert space fragmentation in a driven-dephasing Rydberg atom array

Tianyi Yan,[*] Chun Hei Leung, and Weibin Li
School of Physics and Astronomy and Centre for the Mathematics and Theoretical Physics of Quantum Nonequilibrium Systems, University of Nottingham, Nottingham NG7 2RD, United Kingdom

(Received 19 December 2025; accepted 25 June 2026; published 28 July 2026)

We investigate the onset and mechanism of Hilbert space fragmentation (HSF) in a chain of strongly interacting Rydberg atoms subjected to local dephasing. It is found that the emergence of multiple long-lived metastable states is fundamentally tied to the HSF of the driven-dephasing Rydberg atom system. We demonstrate that the dephasing PXP model, the effective constrained model for strongly blockaded Rydberg atoms, captures the manifesting HSF and supports multiple degenerate zero modes. These modes form disconnected block-diagonal subspaces of maximally mixed states, which consist of many-body spin states sharing the same symmetry. A key result is the identification of the underlying symmetry in the HSF, where the conserved quantities in each subspace are defined by the consecutive double excitation addressing operator. Moreover, we show explicitly that the number of fragmented Hilbert spaces grows exponentially with the chain length, following a modified Fibonacci sequence. Our work provides insights into many-body dynamics under dynamical constraints and opens avenues for controlling and manipulating HSF in Rydberg atom systems.

DOI: 10.1103/691w-6cx8

Introduction. Dynamical constraints can break Hilbert spaces of a many-body system into disconnected subsectors [1–3], leading to Hilbert space fragmentation (HSF) [4–7]. Dynamics confined in a subspace depends sensitively on the symmetry and initial states. A celebrated paradigm is the PXP and related models [8–19], which have been demonstrated with Rydberg atoms [20,21]. The interaction-induced dipole blockade between the Rydberg atoms generates the dynamical constraint [22,23]. Though the resulting dynamics generally thermalize and obey the eigenstate thermalization hypothesis [24–28], initial states that overlap strongly with quantum many-body scars lead to weakly broken ergodicity [29,30]. As a result, nonthermal, oscillatory dynamics takes place in the many-body scar subspace [7,31–36]. On the other hand, the disconnected subspace can thermalize within its small, specific fragment. The resulting Krylov restricted thermalization [1,2,5–7,37–51] has been demonstrated with cold atoms [52,53], superconducting circuits [54], and Rydberg atom arrays [55]. In open quantum systems, the interplay between dynamical constraints and dissipation leads to a competition between retaining and losing information about the initial states, significantly altering the dynamics. Inspired by this perspective, recent studies have shown the stabilization of entangled stationary states in the Temperley-Lieb model [56], stationary states in the East-West model [57], and the generation of dissipative time crystals [58]. Open quantum systems typically relax to a unique steady state independent of the initial condition. How dynamical constraints generate HSF out of the steady state remains largely unexplored.

In this work, we investigate the emergence of HSF in the dynamics of a chain of strongly interacting Rydberg atoms under local dephasing, as illustrated in Fig. 1(a). The resulted Rydberg blockade drastically affects the dissipative dynamics, such that different initial states evolve into distinguishable metastable states before thermalizing into the unique stationary state in the long time limit [Fig. 1(b)]. We show that multiple metastable states arise from HSF, with their dynamics captured by an effective dephasing PXP model. Uniquely, the effective model supports a large number of degenerate zero modes (stationary states) that form disconnected Hilbert subspaces [Fig. 1(c)]. Using a consecutive double excitation addressing operator, we classify the subspaces into classes with conserved symmetries. Dynamics starting from one subspace is entirely confined to the subspace, corresponding to the metastable states of the Rydberg atom chain. We find that the number of Hilbert subspaces is determined by a modified Fibonacci sequence, $f(L) = f(L-1) + f(L-2) + f(L-4)$, and grows exponentially with L. Our study offers insights into the understanding and control of HSF in the dissipative regime within the Rydberg atom array platform. This provides a pathway for exploring constrained dynamics, such as strong fragmentation and metastability, across different subspaces.

Driven-dephasing Rydberg atom chain. Our system is a chain of L atoms, where the atoms are laser-addressed individually [59,60]. As shown in Fig. 1(a), atoms in the electronic ground state $|0\rangle$ resonantly couple to the Rydberg state $|1\rangle$ with Rabi frequency Ω. In the Rydberg state, the jth and kth atoms interact strongly via the van der Waals (vdW) interaction $V_{jk} = V/|j-k|^6$ [22,23], where $V = C_6/a^6$ is the nearest-neighbor (NN) interaction with C_6 and a to be the dispersion coefficient and spacing between

[*]Contact author: tianyi.yan@nottingham.ac.uk

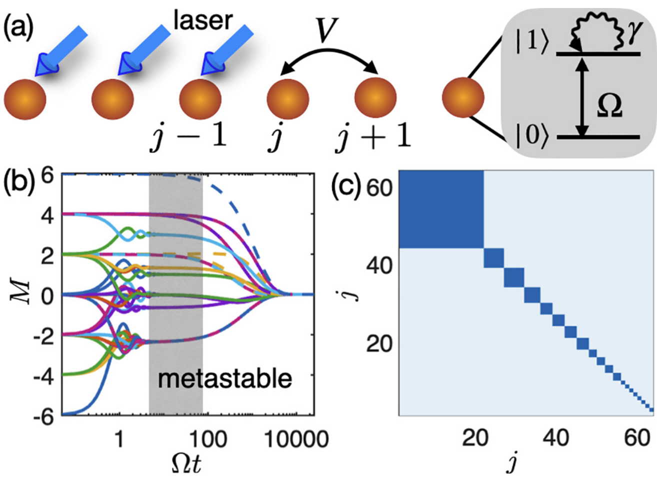

FIG. 1. (a) Atom array and energy levels. Atoms are resonantly excited from the ground state $|0\rangle$ to electronically excited Rydberg state $|1\rangle$ by a laser field (Rabi frequency Ω). In the Rydberg state, atoms experience a dephasing with rate γ. The strong van der Waals interaction [V is the NN interaction] between Rydberg atoms leads to dynamical constraints. (b) Metastable dynamics. The total magnetization M exhibits a metastable evolution on the intermediate timescale $1 \lesssim \Omega t \lesssim 100$ (shaded). The metastable dynamics is effectively described by the dephasing PXP model. (c) In the metastable regime, the Hilbert space is fragmented into many disconnected subspaces, corresponding to the degenerate zero modes of the dephasing PXP model. Index j is the decimal number converted from the binary representation of the basis, as given in Table I. In panel (b), we consider $V = 50\Omega$, $L = 6$, and $\gamma = 2\Omega$. See text for details.

neighboring sites, respectively. The dynamics of the atom is described by a many-body spin Hamiltonian ($\hbar \equiv 1$), $H_o = \Omega \sum_{j=1}^{L} \sigma_j^x + \sum_{j<k}^{L} V_{jk} Q_j Q_k$, where $\sigma_j^x = |1\rangle_j\langle 0| + |0\rangle_j\langle 1|$ and $Q_j = |1\rangle_j\langle 1|$ are the Pauli and projection operators in the jth site.

In the Rydberg state $|1\rangle$, atoms are subject to local dephasing due to laser noise and the residual Doppler effect [61,62]. Density matrix ρ_o of the many-atom system is governed by a Lindblad master equation, $\partial_t \rho_o = \tilde{\mathcal{L}}(\rho_o)$, where Liouvillian $\tilde{\mathcal{L}}(\rho_o)$ reads

$$\tilde{\mathcal{L}}(\rho_o) = -i[H_o, \rho_o] + \mathcal{D}(\rho_o), \tag{1}$$

with $\mathcal{D}(\rho_o) = \gamma \sum_{j=1}^{L} (Q_j \rho_o Q_j^\dagger - \frac{1}{2}\{Q_j^\dagger Q_j, \rho_o\})$ describing the dephasing (rate γ). The local dephasing eliminates the coherence of the system, such that the state equilibrates to the maximally mixed state $\rho_\infty = \mathbb{I}/D$ in the limit $t \to \infty$, where $\mathbb{I}$ and $D = 2^L$ are the identity matrix and dimension of the Hilbert space, respectively [63]. However, the dynamics toward stationarity relies crucially on the interplay among vdW interactions, dephasing, and laser coupling. In the strongly dephasing regime $\gamma \gg |\Omega|$, previous studies have shown critical and universal behaviors in random gases of Rydberg atoms [63–69]. Dynamical constraints driven by the interplay progressively slow down the relaxation processes to the stationary state [64]. In contrast, we explore the HSF emerging in the neutral atom chain in the *strong interaction* regime.

Metastable nonthermal dynamics and fragmentation. When $V \gg \{\Omega,\ \gamma\}$, the generic behavior of the driven-dephasing dynamics is that memories of initial states are retained for extended periods of time. We illustrate this by investigating dynamics of total magnetization $M = \mathrm{Tr}(\rho_o \sum_j \sigma_j^z)$. Initially, the atom chain is prepared in spin basis states along the z direction, $|s_1 s_2 \cdots s_L\rangle$, with $s_j = 0$ or 1 denoting spin states in site j. At $t = 0$, $M = -L, -L+2, \ldots, L$, which gives the number differences of the spin states in the basis. By using each spin basis as the initial state individually, we numerically solve the ME and evaluate M for moderate L. To be concrete, we consider a chain of $L = 6$ atoms with parameters $V = 50\Omega$ and $\gamma = 2\Omega$. As shown in Fig. 1(b), striking features are observed in the dynamics.

First, M remains unchanged over the intermediate timescale, resulting in the formation of metastable phases [shaded region in Fig. 1(b)] [70]. When the initial state is approximately a frozen state of the Liouvillian [71], M is constant up to $\Omega t \approx 100$ (dashed). As a result, the purity of the state is high, $P = \mathrm{Tr}\rho_o^2 \approx 1$, as shown in Fig. 2(a). In other cases, M attains a quasistationary value over an interval $1 \lesssim \Omega t \lesssim 100$. The same is found for the purity of the system. In both cases, the duration of the metastable phase is much longer than the characteristic dephasing time $1/\gamma$ [72–74]. Further discussions and examples of metastable dynamics are provided in the Supplemental Material [75]. Notably, the metastable dynamics relies crucially on the dephasing. When $\gamma = 0$, M becomes highly oscillatory except from the frozen state [Fig. 2(b)] and loses the metastable profiles.

Second, the metastable timescale is encoded in the complex eigenspectrum λ_j of the Liouvillian $\tilde{\mathcal{L}}(\cdot)$. As shown in Fig. 2(c), most of the eigenmodes have large real parts [$|\mathrm{Re}(\lambda_j)| > \gamma$], which determine the transient dynamics. However, 20 modes have near degenerate complex energies close to 0, i.e., $\mathrm{Im}(\lambda_j) = 0$ [Fig. 2(c)] and $|\mathrm{Re}(\lambda_j)| \ll \gamma$ [Fig. 2(d1)]. The very small $|\mathrm{Re}(\lambda_j)|$ shows that the quasidegenerate modes decay slowly and result to the metastable dynamics. For example, the decay rate of the longest metastable dynamics is determined by the spectral gap (smallest nonzero $|\mathrm{Re}(\lambda_j)|$). As illustrated in the Supplemental Material [75], the decay rate and gap are in good agreement. To understand the parameter dependence of the gap, an effective decay rate, $\gamma_{\mathrm{mf}} = \Omega^2\gamma/V^2$, is obtained through a mean field calculation [64,75]. Apparently, $\gamma_{\mathrm{mf}} \ll \gamma$ in the strong interaction regime $V \gg \Omega$. In Fig. 2(d2), γ_{mf} and the Liouvillian gap up to $L = 13$ are shown. The gap gradually approaches γ_{mf} when L increases. This trend indicates that the metastable dynamics is robust even for large system sizes.

Finally, the metastable plateaus themselves depend on the chosen initial state, exhibiting a memory effect. We find nine plateaus in the magnetization [Fig. 1(b)] and six in purity [Fig. 2(a)] that are isolated from their neighbors, although some of them can have the same initial values. These numbers are significantly smaller than Hilbert space dimension $D = 64$. In the following, we will reveal that the memory effect and clustering of the observable are rooted in the Hilbert (Krylov) space fragmentation [1].

Liouvillian zero modes and Hilbert space fragmentation of the dephasing PXP model. To derive the effective model, we make use of a unitary transformation $U = e^{-iVt\sum_j Q_j Q_{j+1}}$.

TABLE I. Representative basis and their equivalence classes. Here P, M, and $\mathcal{A}$ are expectation values of the purity, magnetization, and CDEA operator, repectively. The chain length is $L = 6$.

$\boldsymbol{P}$	M	$\langle\mathcal{A}\rangle$	Rep	Equivalence class
$\frac{1}{21}$	$-\frac{50}{21}$	0	$\|000000\rangle$	$\{\|000000\rangle, \|000001\rangle, \|000010\rangle, \|000100\rangle, \|000101\rangle, \|001000\rangle, \|001001\rangle, \|001010\rangle, \|010000\rangle, \|010001\rangle, \|010010\rangle, \|010100\rangle, \|010101\rangle, \|100000\rangle, \|100001\rangle, \|100010\rangle, \|100100\rangle, \|100101\rangle, \|101000\rangle, \|101001\rangle, \|101010\rangle\}$
$\frac{1}{5}$	0	2	$\|110000\rangle$	$\{\|110000\rangle, \|110001\rangle, \|110010\rangle, \|110100\rangle, \|110101\rangle\}$
	0	32	$\|000011\rangle$	$\{\|000011\rangle, \|001011\rangle, \|010011\rangle, \|100011\rangle, \|101011\rangle\}$
$\frac{1}{4}$	0	8	$\|001100\rangle$	$\{\|001100\rangle, \|001101\rangle, \|101100\rangle, \|101101\rangle\}$
$\frac{1}{3}$	$-\frac{2}{3}$	4	$\|011000\rangle$	$\{\|011000\rangle, \|011001\rangle, \|011010\rangle\}$
	$\frac{4}{3}$	6	$\|111000\rangle$	$\{\|111000\rangle, \|111001\rangle, \|111010\rangle\}$
	$-\frac{2}{3}$	16	$\|000110\rangle$	$\{\|000110\rangle, \|010110\rangle, \|100110\rangle\}$
	$\frac{4}{3}$	48	$\|000111\rangle$	$\{\|000111\rangle, \|010111\rangle, \|100111\rangle\}$
$\frac{1}{2}$	1	12	$\|011100\rangle$	$\{\|011100\rangle, \|011101\rangle\}$
	3	14	$\|111100\rangle$	$\{\|111100\rangle, \|111101\rangle\}$
	1	24	$\|001110\rangle$	$\{\|001110\rangle, \|101110\rangle\}$
	3	56	$\|001111\rangle$	$\{\|001111\rangle, \|101111\rangle\}$
1	2	18	$\|110110\rangle$	$\{\|110110\rangle\}$
	2	28	$\|011110\rangle$	$\{\|011110\rangle\}$
	4	30	$\|111110\rangle$	$\{\|111110\rangle\}$
	2	34	$\|110011\rangle$	$\{\|110011\rangle\}$
	2	36	$\|011011\rangle$	$\{\|011011\rangle\}$
	4	38	$\|111011\rangle$	$\{\|111011\rangle\}$
	4	50	$\|110111\rangle$	$\{\|110111\rangle\}$
	4	60	$\|011111\rangle$	$\{\|011111\rangle\}$
	6	62	$\|111111\rangle$	$\{\|111111\rangle\}$

In the strong interaction limit, the transformation leads to the PXP Hamiltonian $H_{\rm PXP} = \Omega \sum_{j=2}^{L-1} P_{j-1}\sigma_j^x P_{j+1}$ [10,34,76]. In deriving $H_{\rm PXP}$, we have neglected fast oscillating terms and kept only the NN interaction [75]. Interestingly, longer range interactions do not affect the underlying HSF. This will become evident when we discuss the symmetry of the Liouvillian in the following section and in the Supplemental Material [75]. Using the fact that this transformation does not affect the dephasing operators in Eq. (1), we obtain the dephasing PXP (dPXP) model, governed by Liouvillian $\mathcal{L}(\rho) = -i[H_{\rm PXP}, \rho] + \mathcal{D}(\rho)$, with $\rho = U^\dagger \rho_{\rm o} U$. We will show that the dPXP model not only captures the metastable dynamics, but also provides important insights into the fragmentation.

To illustrate the accuracy, we first calculate the magnetization and purity with the dPXP model, and show the result in Figs. 2(e)–2(g). Both the magnetization and purity are restricted to special values, which agree with the data shown in Figs. 2(a) and 2(b) up to $\Omega t \approx 100$. When $\Omega t > 100$, the values obtained from the dPXP model remain invariant with time and depend only on the initial state. The complex spectra of the dPXP model are then calculated numerically and shown in Fig. 2(g). Central to the spectra is the presence of 21 degenerate zero modes, whose eigenvalues have zero real parts [Fig. 2(g)]. Each mode is a maximally mixed state $\rho_d = \mathbb{I}_d/d$ in the spin basis representation, where d is the dimension of the respective Hilbert subspace. These zero modes form a series of *disconnected Hilbert subspaces*, giving rise to the HSF. The memory effect arises in the dynamics such that the initial states that fall in different subspaces do not influence each other [see Figs. 2(e) and 2(f)].

The classical nature of the zero modes permits the iterative construction of the Hilbert subspace. This is done by starting from a basis and applying $H_{\rm PXP}$ to the basis repeatedly. This process identifies basis states linked to the initial state, which collectively form a subspace, also referred to as an equivalence class. For each class, we select a representative basis state that has the smallest decimal value when converted from its binary representation. The procedure is then repeated by selecting a new basis that is not part of the previously identified subspace. This approach explicitly and systematically finds all the equivalence classes. In Table I, we present the equivalence classes and their corresponding representatives for $L = 6$. The largest equivalent class consists of basis that form the quantum many-body scar states. They allow us to construct the fragmented Hilbert space for the dPXP model, as shown in Fig. 1(c).

Both the purity and magnetization can be evaluated once the class is determined. If a class consists of multiple basis

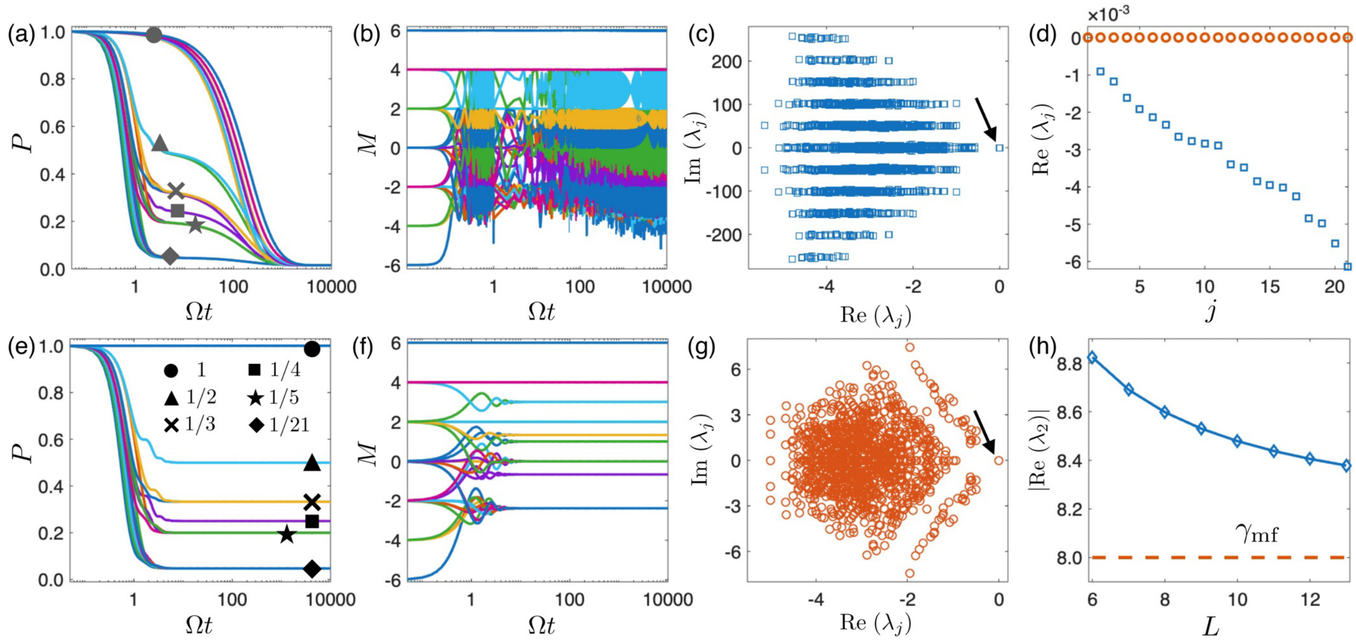

FIG. 2. Metastable dynamics, zero mode, and fragmentation. (a) Purity of the atom chain. ρ_o is largely pure in the metastable state when starting from the frozen state (marked with a filled circle). Other basis states partially retain coherence in the metastable dynamics (filled labels). (b) Magnetization M in a dephasing free Rydberg atom chain. Outside the frozen states, the magnetization of the different subspaces rapidly oscillates over time. This overlap makes it difficult to discern the dependence on the initial states. (c) Complex spectrum of Liouvillian $\tilde{\mathcal{L}}$. There are 20 nearly degenerate modes (arrow) around the stationary mode ($\lambda_j = 0$). (d1) Real parts $\mathrm{Re}(\lambda_j)$ of the quasidegenerate (square) and degenerate (circle) modes. (d2) Scaling of the gap $|\mathrm{Re}(\lambda_2)|$ with L. As L increases, the gap decreases and approaches the mean field result γ_{mf}. (e) Purity of the dPXP model. The steady P is determined by the dimensions of the respective subspace, as marked in the figure. In panel (a), the purity in the metastable state is close to that of the dPXP model. The purity of the frozen states is 1. (f) Magnetization of the dPXP model. Owing to fragmentation, M does not change with time after the initial transient period (solid). In the frozen state, M is constant. (g) Complex spectra of the Liouvillian $\mathcal{L}(\rho)$. There are 21 degenerate zero modes, the real parts of which are shown in panel (d1). Here, $V = 50\Omega$ in panels (a)–(d). Other parameters are given in Fig. 1.

states, its stationary purity is determined by the dimension d of the subspace, $P(t \to \infty) = 1/d$, which is listed in Table I for different classes. There is a special group, where each class contains a single basis (bottom of Table I). This basis alone is a zero mode. In other words, they are the so-called frozen states in the dynamical evolution, where the observable is invariant with time [71]. For $L = 6$, the nine frozen states are $|011011\rangle$, $|011110\rangle$, $|011111\rangle$, $|110011\rangle$, $|110110\rangle$, $|110111\rangle$, $|111011\rangle$, $|111110\rangle$, and $|111111\rangle$. Similarly, the magnetization can be determined analytically in each class, as given in Table I. The analytical results match those of the numerical results [Fig. 1(b)].

Strong symmetry and scaling of the HSF. The symmetry of the Liouvillian can be defined with the consecutive double excitations addressing (CDEA) operator,

$$\mathcal{A} = \sum_{j=1}^{L-1} 2^j Q_j Q_{j+1}, \tag{2}$$

which is the weighted sum of consecutive double excitations (given by the adjoint projection operator $Q_j Q_{j+1}$) along the spin chain. Each pair is assigned a unique weight 2^j according to its position in the chain (from left to right). The CDEA operator commutes with the PXP Hamiltonian and every dephasing operator, i.e., $[H_{\mathrm{PXP}}, \mathcal{A}] = 0$ and $[\mathcal{A}, Q_j] = 0\ \forall j$. Hence, it acts as a strong symmetry of the Liouvillian $\mathcal{L}$ [56].

We find $\langle\mathcal{A}\rangle = 0$ in the largest equivalent class, in which no consecutive double excitation is permitted. The corresponding basis forms the quantum many-body scar states. It is noteworthy that the operator $\mathcal{A}$ commutes with the longer-range interaction parts in H_o. This justifies the omission of these terms in deriving the dPXP model, as they do not influence the symmetry. Although the Hamiltonian H_{PXP} preserves the symmetry, other observables, such as magnetization, oscillate with time. The dynamical evolution of different classes could overlap temporally, as depicted in Fig. 2(b). In contrast, identifying consecutive double excitations and other related observable is straightforward in a stationary state of the Liouvillian.

The expectation value $\langle\mathcal{A}\rangle$ of the equivalence class is given in Table I. Each class has a unique expectation value, such that the CDEA operator identifies the symmetry of the fragmented subspace. We note that the CDEA operator approximately preserves strong symmetry in the Rydberg atom chain system. In Fig. 3(a), dynamical evolution of the expectation value $\langle\mathcal{A}\rangle_o = \mathrm{Tr}(\rho_o\mathcal{A})$ is shown. It is a constant and coincides with the corresponding $\langle\mathcal{A}\rangle$, before converging to the thermal value $\langle\mathcal{A}\rangle_\infty = \mathrm{Tr}(\rho_\infty\mathcal{A}) = 31/2$. For arbitrary L, the thermal value $\langle\mathcal{A}\rangle_\infty = 2^{L-2} - 1/2$ [75]. Furthermore, the spontaneous decay (rate γ_{dec}) in the Rydberg state can be largely neglected, provided that $\gamma_{\mathrm{mf}} > \gamma_{\mathrm{dec}}$. This condition permits the metastable dynamics to occur prior to the decay.

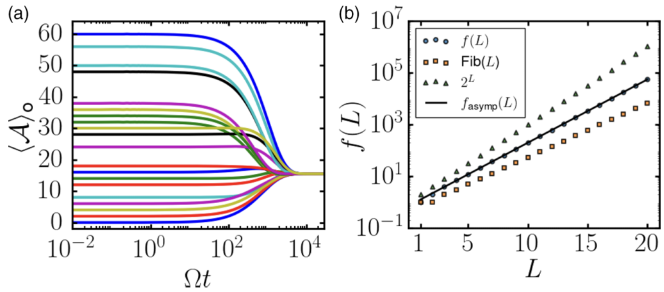

FIG. 3. (a) Dynamics of $\langle\mathcal{A}\rangle_o$. In the metastable regime ($\Omega t \leqslant 100$), the CDEA operator is almost constant. The parameters are the same as those in Fig. 2. (b) Number $f(L)$ of zero modes with respect to chain length L. As shown by the solid line, $f(L)$ increases with L exponentially. For a given L, $f(L)$ is larger than the Fibonacci sequence (square), but smaller than the Hilbert space dimension $D = 2^L$ (triangle).

Details of the demonstration can be found in the Supplemental Material [75].

Using the commutant algebra [6], we are able to obtain the total number $f(L)$ of the subspaces, which follows a recursive relation [75],

$$f(L) = f(L-1) + f(L-2) + f(L-4), \tag{3}$$

with initial conditions $f(0) = 1$, $f(-1) = 1$, $f(-2) = 0$, and $f(-3) = -1$. Importantly, $f(L)$ scales with L exponentially when L is large [75],

$$f_{\rm asymp}(L) \approx A\alpha^L, \tag{4}$$

where $A \approx 0.722\,124$ and $\alpha \approx 1.754\,877$. As shown in Fig. 3(b), the scaling agrees with the exact $f(L)$ well. It is different from the Fibonacci sequence due to the $f(L-4)$ term. In fact, it surpasses scaling of the Fibonacci sequence $\mathrm{F}(L) \approx \varphi^L/\sqrt{5}$ with $\varphi = (1+\sqrt{5})/2$ to be the golden ratio. Despite the exponential scaling, the total number of the subspaces is significantly smaller than the total Hilbert space dimension D [Fig. 3(b)].

Conclusion. We have investigated the HSF in a chain of strongly interacting Rydberg atoms under local dephasing. The onset of the metastable HSF is captured effectively by the dPXP model. The multiple, degenerate zero modes of the dPXP model form the fragmented Hilbert subspace. Using the CDEA operator, we have classified the zero modes and identified the basis states that compose the zero modes. The number of the zero modes, given by the modified Fibonacci sequence, grows exponentially with the chain length. The many-body scar states within the PXP Hamiltonian constitutes the largest subspace in the dPXP model. Our study offers a detailed classification of the entire Hilbert space, while the dephasing process stabilizes the subspaces into the zero modes of the Liouvillian. Benefited from the precise control of the coherent [55,59,60] and dissipative couplings [77,78], our study paves a route to investigate the dissipative fragmentation and emerging dynamically constrained dynamics, such as entanglement and correlation in the fragmented Hilbert space [56,58,79], and competition between localization and fragmentation in the presence of noises (e.g., in Rabi frequency or laser detuning) [80], with the state-of-the-art Rydberg atom simulator [59,60].

Acknowledgments. We thank Stephen Powell, Juan Garrahan, Masud Haque, Kay Brandner, Arash Jafarizadeh, Jonas Glatthard, Konstantinos Sfairopoulos, and Yuqiang Liu for helpful discussion. We acknowledge support from the EPSRC through Grants No. EP/W015641/1 and No. EP/W524402/1, and the use of the University of Nottingham's Ada HPC service.

Data availability. The data that support the findings of this study are openly available [81].

[1] P. Sala, T. Rakovszky, R. Verresen, M. Knap, and F. Pollmann, Ergodicity breaking arising from Hilbert space fragmentation in dipole-conserving Hamiltonians, Phys. Rev. X **10**, 011047 (2020).

[2] V. Khemani, M. Hermele, and R. Nandkishore, Localization from Hilbert space shattering: From theory to physical realizations, Phys. Rev. B **101**, 174204 (2020).

[3] S. Roy and A. Lazarides, Strong ergodicity breaking due to local constraints in a quantum system, Phys. Rev. Res. **2**, 023159 (2020).

[4] Z.-C. Yang, F. Liu, A. V. Gorshkov, and T. Iadecola, Hilbert-space fragmentation from strict confinement, Phys. Rev. Lett. **124**, 207602 (2020).

[5] D. Hahn, P. A. McClarty, and D. J. Luitz, Information dynamics in a model with Hilbert space fragmentation, SciPost Phys. **11**, 074 (2021).

[6] S. Moudgalya and O. I. Motrunich, Hilbert space fragmentation and commutant algebras, Phys. Rev. X **12**, 011050 (2022).

[7] S. Moudgalya, B. A. Bernevig, and N. Regnault, Quantum many-body scars and Hilbert space fragmentation: A review of exact results, Rep. Prog. Phys. **85**, 086501 (2022).

[8] R. Moessner and S. L. Sondhi, Ising models of quantum frustration, Phys. Rev. B **63**, 224401 (2001).

[9] P. Fendley, K. Sengupta, and S. Sachdev, Competing density-wave orders in a one-dimensional hard-boson model, Phys. Rev. B **69**, 075106 (2004).

[10] I. Lesanovsky, Many-body spin interactions and the ground state of a dense Rydberg lattice gas, Phys. Rev. Lett. **106**, 025301 (2011).

[11] V. Khemani, C. R. Laumann, and A. Chandran, Signatures of integrability in the dynamics of Rydberg-blockaded chains, Phys. Rev. B **99**, 161101(R) (2019).

[12] S. Choi, C. J. Turner, H. Pichler, W. W. Ho, A. A. Michailidis, Z. Papić, M. Serbyn, M. D. Lukin, and D. A. Abanin, Emergent SU(2) dynamics and perfect quantum many-body scars, Phys. Rev. Lett. **122**, 220603 (2019).

[13] C.-J. Lin, A. Chandran, and O. I. Motrunich, Slow thermalization of exact quantum many-body scar states under perturbations, Phys. Rev. Res. **2**, 033044 (2020).
[14] R. Verresen, M. D. Lukin, and A. Vishwanath, Prediction of toric code topological order from Rydberg blockade, Phys. Rev. X **11**, 031005 (2021).
[15] V. Karle, M. Serbyn, and A. A. Michailidis, Area-law entangled eigenstates from nullspaces of local Hamiltonians, Phys. Rev. Lett. **127**, 060602 (2021).
[16] F. M. Surace, M. Votto, E. G. Lazo, A. Silva, M. Dalmonte, and G. Giudici, Exact many-body scars and their stability in constrained quantum chains, Phys. Rev. B **103**, 104302 (2021).
[17] G.-X. Su, H. Sun, A. Hudomal, J.-Y. Desaules, Z.-Y. Zhou, B. Yang, J. C. Halimeh, Z.-S. Yuan, Z. Papić, and J.-W. Pan, Observation of many-body scarring in a Bose-Hubbard quantum simulator, Phys. Rev. Res. **5**, 023010 (2023).
[18] A. N. Ivanov and O. I. Motrunich, Volume-entangled exact scar states in the PXP and related models in any dimension, Phys. Rev. Lett. **134**, 050403 (2025).
[19] A. Kerschbaumer, M. Ljubotina, M. Serbyn, and J.-Y. Desaules, Quantum many-body scars beyond the PXP model in Rydberg simulators, Phys. Rev. Lett. **134**, 160401 (2025).
[20] H. Bernien, S. Schwartz, A. Keesling, H. Levine, A. Omran, H. Pichler, S. Choi, A. S. Zibrov, M. Endres, M. Greiner, V. Vuletić, and M. D. Lukin, Probing many-body dynamics on a 51-atom quantum simulator, Nature (London) **551**, 579 (2017).
[21] D. Bluvstein, A. Omran, H. Levine, A. Keesling, G. Semeghini, S. Ebadi, T. T. Wang, A. A. Michailidis, N. Maskara, W. W. Ho, S. Choi, M. Serbyn, M. Greiner, V. Vuletić, and M. D. Lukin, Controlling quantum many-body dynamics in driven Rydberg atom arrays, Science **371**, 1355 (2021).
[22] M. Saffman, T. G. Walker, and K. Mølmer, Quantum information with Rydberg atoms, Rev. Mod. Phys. **82**, 2313 (2010).
[23] X.-Q. Shao, S.-L. Su, L. Li, R. Nath, J.-H. Wu, and W. Li, Rydberg superatoms: An artificial quantum system for quantum information processing and quantum optics, Appl. Phys. Rev. **11**, 031320 (2024).
[24] J. M. Deutsch, Quantum statistical mechanics in a closed system, Phys. Rev. A **43**, 2046 (1991).
[25] M. Srednicki, Chaos and quantum thermalization, Phys. Rev. E **50**, 888 (1994).
[26] M. Rigol, V. Dunjko, and M. Olshanii, Thermalization and its mechanism for generic isolated quantum systems, Nature (London) **452**, 854 (2008).
[27] A. Polkovnikov, K. Sengupta, A. Silva, and M. Vengalattore, Colloquium: Nonequilibrium dynamics of closed interacting quantum systems, Rev. Mod. Phys. **83**, 863 (2011).
[28] L. D'Alessio, Y. Kafri, A. Polkovnikov, and M. Rigol, From quantum chaos and eigenstate thermalization to statistical mechanics and thermodynamics, Adv. Phys. **65**, 239 (2016).
[29] R. G. Palmer, D. L. Stein, E. Abrahams, and P. W. Anderson, Models of hierarchically constrained dynamics for glassy relaxation, Phys. Rev. Lett. **53**, 958 (1984).
[30] G. H. Fredrickson and H. C. Andersen, Kinetic Ising model of the glass transition, Phys. Rev. Lett. **53**, 1244 (1984).
[31] C. J. Turner, A. A. Michailidis, D. A. Abanin, M. Serbyn, and Z. Papić, Weak ergodicity breaking from quantum many-body scars, Nat. Phys. **14**, 745 (2018).
[32] C. J. Turner, A. A. Michailidis, D. A. Abanin, M. Serbyn, and Z. Papić, Quantum scarred eigenstates in a Rydberg atom chain: Entanglement, breakdown of thermalization, and stability to perturbations, Phys. Rev. B **98**, 155134 (2018).
[33] C.-J. Lin and O. I. Motrunich, Exact quantum many-body scar states in the Rydberg-blockaded atom chain, Phys. Rev. Lett. **122**, 173401 (2019).
[34] M. Serbyn, D. A. Abanin, and Z. Papić, Quantum many-body scars and weak breaking of ergodicity, Nat. Phys. **17**, 675 (2021).
[35] Z. Yao, L. Pan, S. Liu, and H. Zhai, Quantum many-body scars and quantum criticality, Phys. Rev. B **105**, 125123 (2022).
[36] A. Chandran, T. Iadecola, V. Khemani, and R. Moessner, Quantum many-body scars: A quasiparticle perspective, Annu. Rev. Condens. Matter Phys. **14**, 443 (2023).
[37] G. De Tomasi, D. Hetterich, P. Sala, and F. Pollmann, Dynamics of strongly interacting systems: From Fock-space fragmentation to many-body localization, Phys. Rev. B **100**, 214313 (2019).
[38] S. Moudgalya, A. Prem, R. Nandkishore, N. Regnault, and B. A. Bernevig, Thermalization and its absence within Krylov subspaces of a constrained Hamiltonian, in *Memorial Volume for Shoucheng Zhang*, edited by B. Lian, C. X. Liu, E. Demler, S. Kivelson, and X. Qi (World Scientific, Singapore, 2021), p. 147.
[39] C. M. Langlett and S. Xu, Hilbert space fragmentation and exact scars of generalized Fredkin spin chains, Phys. Rev. B **103**, L220304 (2021).
[40] B. Pozsgay, T. Gombor, A. Hutsalyuk, Y. Jiang, L. Pristyák, and E. Vernier, Integrable spin chain with Hilbert space fragmentation and solvable real-time dynamics, Phys. Rev. E **104**, 044106 (2021).
[41] E. V. H. Doggen, I. V. Gornyi, and D. G. Polyakov, Stark many-body localization: Evidence for Hilbert-space shattering, Phys. Rev. B **103**, L100202 (2021).
[42] T. Rakovszky, P. Sala, R. Verresen, M. Knap, and F. Pollmann, Statistical localization: From strong fragmentation to strong edge modes, Phys. Rev. B **101**, 125126 (2020).
[43] B. Mukherjee, D. Banerjee, K. Sengupta, and A. Sen, Minimal model for Hilbert space fragmentation with local constraints, Phys. Rev. B **104**, 155117 (2021).
[44] T. Kohlert, S. Scherg, P. Sala, F. Pollmann, B. Hebbe Madhusudhana, I. Bloch, and M. Aidelsburger, Exploring the regime of fragmentation in strongly tilted Fermi-Hubbard chains, Phys. Rev. Lett. **130**, 010201 (2023).
[45] E. Nicolau, A. M. Marques, J. Mompart, V. Ahufinger, and R. G. Dias, Local Hilbert space fragmentation and weak thermalization in Bose-Hubbard diamond necklaces, Phys. Rev. B **107**, 094312 (2023).
[46] G. Francica and L. Dell'Anna, Hilbert space fragmentation in a long-range system, Phys. Rev. B **108**, 045127 (2023).
[47] P. Brighi, M. Ljubotina, and M. Serbyn, Hilbert space fragmentation and slow dynamics in particle-conserving quantum East models, SciPost Phys. **15**, 093 (2023).
[48] R. J. Valencia-Tortora, N. Pancotti, M. Fleischhauer, H. Bernien, and J. Marino, Rydberg platform for nonergodic chiral quantum dynamics, Phys. Rev. Lett. **132**, 223201 (2024).
[49] S. Aditya, D. Dhar, and D. Sen, Subspace-restricted thermalization in a correlated-hopping model with strong Hilbert space fragmentation characterized by irreducible strings, Phys. Rev. B **110**, 045418 (2024).

[50] M. Ganguli, S. Aditya, and D. Sen, Aspects of Hilbert space fragmentation in the quantum East model: Fragmentation, subspace-restricted quantum scars, and effects of density-density interactions, Phys. Rev. B **111**, 045411 (2025).

[51] F. Yang, H. Yarloo, H.-C. Zhang, K. Mølmer, and A. E. B. Nielsen, Probing Hilbert space fragmentation with strongly interacting Rydberg atoms, Phys. Rev. B **111**, 144313 (2025).

[52] D. Adler, D. Wei, M. Will, K. Srakaew, S. Agrawal, P. Weckesser, R. Moessner, F. Pollmann, I. Bloch, and J. Zeiher, Observation of Hilbert space fragmentation and fractonic excitations in 2D, Nature (London) **636**, 80 (2024).

[53] K. Honda, Y. Takasu, S. Goto, H. Kazuta, M. Kunimi, I. Danshita, and Y. Takahashi, Observation of slow relaxation due to Hilbert space fragmentation in strongly interacting Bose-Hubbard chains, Sci. Adv. **11**, eadv3255 (2025).

[54] Y.-Y. Wang *et al.*, Exploring Hilbert-space fragmentation on a superconducting processor, PRX Quantum **6**, 010325 (2025).

[55] L. Zhao, P. R. Datla, W. Tian, M. M. Aliyu, and H. Loh, Observation of quantum thermalization restricted to Hilbert space fragments and $\mathbb{Z}_{2k}$ scars, Phys. Rev. X **15**, 011035 (2025).

[56] Y. Li, P. Sala, and F. Pollmann, Hilbert space fragmentation in open quantum systems, Phys. Rev. Res. **5**, 043239 (2023).

[57] A. Marché, G. Morettini, L. Mazza, L. Gotta, and L. Capizzi, Exceptional stationary state in a dephasing many-body open quantum system, Phys. Rev. Lett. **135**, 020406 (2025).

[58] H. Li and W. Yi, Symmetry-induced fragmentation and dissipative time crystal, Phys. Rev. B **113**, 014316 (2026).

[59] A. Browaeys and T. Lahaye, Many-body physics with individually controlled Rydberg atoms, Nat. Phys. **16**, 132 (2020).

[60] S. Ebadi, T. T. Wang, H. Levine, A. Keesling, G. Semeghini, A. Omran, D. Bluvstein, R. Samajdar, H. Pichler, W. W. Ho, S. Choi, S. Sachdev, M. Greiner, V. Vuletić, and M. D. Lukin, Quantum phases of matter on a 256-atom programmable quantum simulator, Nature (London) **595**, 227 (2021).

[61] J. Honer, R. Löw, H. Weimer, T. Pfau, and H. P. Büchler, Artificial atoms can do more than atoms: Deterministic single photon subtraction from arbitrary light fields, Phys. Rev. Lett. **107**, 093601 (2011).

[62] S. Helmrich, A. Arias, and S. Whitlock, Uncovering the nonequilibrium phase structure of an open quantum spin system, Phys. Rev. A **98**, 022109 (2018).

[63] L. M. Sieberer, M. Buchhold, J. Marino, and S. Diehl, Universality in driven open quantum matter, Rev. Mod. Phys. **97**, 025004 (2025).

[64] I. Lesanovsky and J. P. Garrahan, Kinetic constraints, hierarchical relaxation, and onset of glassiness in strongly interacting and dissipative Rydberg gases, Phys. Rev. Lett. **111**, 215305 (2013).

[65] M. Marcuzzi, E. Levi, S. Diehl, J. P. Garrahan, and I. Lesanovsky, Universal nonequilibrium properties of dissipative Rydberg gases, Phys. Rev. Lett. **113**, 210401 (2014).

[66] M. Hoening, W. Abdussalam, M. Fleischhauer, and T. Pohl, Antiferromagnetic long-range order in dissipative Rydberg lattices, Phys. Rev. A **90**, 021603(R) (2014).

[67] M. Marcuzzi, E. Levi, W. Li, J. P. Garrahan, B. Olmos, and I. Lesanovsky, Non-equilibrium universality in the dynamics of dissipative cold atomic gases, New J. Phys. **17**, 072003 (2015).

[68] S. Helmrich, A. Arias, G. Lochead, T. M. Wintermantel, M. Buchhold, S. Diehl, and S. Whitlock, Signatures of self-organized criticality in an ultracold atomic gas, Nature (London) **577**, 481 (2020).

[69] J. Kazemi and H. Weimer, Driven-dissipative Rydberg blockade in optical lattices, Phys. Rev. Lett. **130**, 163601 (2023).

[70] K. Macieszczak, M. Guţă, I. Lesanovsky, and J. P. Garrahan, Towards a theory of metastability in open quantum dynamics, Phys. Rev. Lett. **116**, 240404 (2016).

[71] H.-P. Breuer and F. Petruccione, *The Theory of Open Quantum Systems* (Oxford University Press, Oxford, UK, 2007).

[72] L.-N. Wu and A. Eckardt, Prethermal memory loss in interacting quantum systems coupled to thermal baths, Phys. Rev. B **101**, 220302 (2020).

[73] S. Saha and R. Bhattacharyya, Prethermalization in an open quantum system coupled to a spatially correlated bosonic bath, J. Stat. Mech. (2024) 023103.

[74] S. Artini, M. Paternostro, and S. Lorenzo, Coherent heat exchange in a prethermalizing open quantum system, Phys. Rev. A **113**, 052203 (2026).

[75] See Supplemental Material at http://link.aps.org/supplemental/10.1103/691w-6cx8 for details on the derivation of the dPXP model, mean field results, recursive relation and scaling of $f(L)$, and dynamics of different chain lengths, which includes Refs. [6,10,57,76].

[76] I. Lesanovsky and H. Katsura, Interacting Fibonacci anyons in a Rydberg gas, Phys. Rev. A **86**, 041601(R) (2012).

[77] T. Chen, C. Huang, J. P. Covey, and B. Gadway, Collective dissipation engineering of interacting Rydberg atoms, arXiv:2509.06373.

[78] Y.-W. Zhang, B. Xu, Y. Zhou, D.-S. Xiang, H.-X. Liu, P. Zhou, K. Zhang, R. Liao, T. Pohl, W. Li, and L. Li, Observation of non-Hermitian many-body phase transition in a Rydberg-atom array, arXiv:2512.02753.

[79] A. Moharramipour, L. A. Lessa, C. Wang, T. H. Hsieh, and S. Sahu, Symmetry-enforced entanglement in maximally mixed states, PRX Quantum **5**, 040336 (2024).

[80] L. Herviou, J. H. Bardarson, and N. Regnault, Many-body localization in a fragmented Hilbert space, Phys. Rev. B **103**, 134207 (2021).

[81] T. Yan, C. Leung, and W. Li, Hilbert space fragmentation in driven-dephasing Rydberg atom array, Zenodo, 2025, https://doi.org/10.5281/zenodo.17769423.